The association of microtubules with tight junctions is promoted by cingulin phosphorylation by AMPK

Tomoki Yano,[1] Takeshi Matsui,[2] Atsushi Tamura,[1] Masami Uji,[1] and Sachiko Tsukita[1]

[1]Laboratory of Biological Science, Graduate School of Frontier Biosciences and Graduate School of Medicine, Osaka University, Osaka 565-0871, Japan
[2]Laboratory for Skin Homeostasis, Research Center for Allergy and Immunology, RIKEN Center for Integrative Medical Sciences, Tsurumi-ku, Yokohama 230-0045, Japan

THE JOURNAL OF CELL BIOLOGY

Epithelial cells characteristically have noncentrosomal microtubules that are arranged in the apicobasal direction. In this paper, we examined cell sheets formed by an epithelial (Eph4) cell line by structure illumination microscopy and found a previously not clearly described planar apical network of noncentrosomal microtubules (MTs) in which the sides of the MT bundles were associated with tight junctions (TJs). In a gel overlay assay with taxol-stabilized MTs, cingulin showed strong binding to MTs, and a domain analysis showed that this binding occurred through cingulin's N-terminal region. The association of planar apical MTs with TJs was compromised by cingulin knockdown (KD) or the expression of dephosphomimetic mutants of cingulin at its adenosine monophosphate–activated protein kinase (AMPK) target sites, whereas phosphorylation at these sites facilitated cingulin–tubulin binding. In addition, although wild-type colonies formed spheres in 3D culture, the cingulin KD cells had anisotropic shapes. These findings collectively suggest that the regulated cingulin–MT association has a specific role in TJ-related epithelial morphogenesis that is sensitive to metabolic homeostasis-related AMPK activity.

Introduction

The structure of epithelial cell sheets, in which cell–cell adhesion is highly organized, is critically dependent on the association of cytoskeletal components with apical cell–cell adhering junctions (including tight junctions [TJs] and adherens junctions [AJs] and desmosomes; Gumbiner, 2000; Tsukita et al., 2001; Perez-Moreno et al., 2003; Franke, 2009; Meng and Takeichi, 2009). Therefore, the dynamic interactions of actin and 10-nm filaments with the plasma membrane at the cell–cell junctions have been well studied in the respect of their roles in organizing cell–cell adhesion/cytoskeleton and in transducing inter- and intracellular signaling (Bornslaeger et al., 1996; Etienne-Manneville and Hall, 2002; Sugimoto et al., 2008; Baum and Georgiou, 2011).

Microtubules (MTs) that interact with plasma membranes are reported to bind MT plus end–tracking proteins at the scaffold in the AJs with their plus ends or to bind Nezha/calmodulin-regulated spectrin-associated proteins and ninein in the AJs with their minus ends (Moss et al., 2007; Shaw et al., 2007; Meng et al., 2008; Meng and Takeichi, 2009). How MTs interact with cell–cell adhering junctions provides clues to how the dynamic arrangements of MTs are regulated in cells. Further analyses of this system should shed light on the molecular bases of the cell–cell junction-based organization of microtubular networks.

Cellular MTs form two types of networks, those composed of centrosomal MTs and those composed of noncentrosomal ones, and the balance between them is thought to be regulated by cell type–dependent cues (Bacallao et al., 1989; Reinsch and Karsenti, 1994; Bartolini and Gundersen, 2006). In epithelial cells, unlike many other cell types, such as fibroblasts, the noncentrosomal MTs dominate; they are oriented apicobasally, although the dynamics of their arrangements have not been well analyzed. Thus, epithelial cell–specific cues likely play a role in their unique MT arrangements. In addition, cell–cell adhesions between epithelial cells are highly organized, particularly in epithelial cell sheets, and the unusual arrangement of MTs may be related to the functions of cell–cell adhering junctions.

The Rockefeller University Press $30.00
J. Cell Biol. Vol. 203 No. 4 605–614
www.jcb.org/cgi/doi/10.1083/jcb.201304194

JCB 605

A potentially fruitful approach to understanding the relationship between the cell–cell adhesion system and MTs' organization in epithelial cell sheets would be to examine the effects of altering cell–cell adhesion system on MT organization. Here, we examined epithelial cell sheets using structured illumination microscopy (SIM) and found a new noncentrosomal MT network, which was organized into a planar apical structures. Furthermore, in addition to associating end-on with the TJs, the MTs were aligned laterally to TJs, with the side of the filaments apparently at the site of the MT–TJ association. We found that the interaction between the MTs and TJs was mediated by cingulin, through its AMP-activated protein kinase (AMPK)–dependent phosphorylation. These results point to the role of the TJ as an organizing site for the apical MT network's formation. When the association of MTs with TJs was perturbed by cingulin knockdown (KD), by expressing dephosphomimetic mutants of cingulin, or by an AMPK inhibitor, the morphogenesis of the cells' 3D colonies was markedly compromised. These findings reveal new information about the distribution and function of the planar apical networks (PANs) of MTs in epithelial cell sheets.

Results and discussion

PANs of noncentrosomal MTs and their lateral association with TJs

Here, we immunostained polarized cell sheets, formed by the Eph4 epithelial cell line, which are derived from the mouse mammary gland, for α-tubulin and ZO-1 (a TJ marker), and observed them by SIM. The results revealed a PAN of noncentrosomal MTs (PAN-MTs), just beneath the apical plasma membrane, at the same level as where the TJs are located (Figs. 1 A and S1 A and Video 1). (In contrast, most of the other noncentrosomal MTs remained aligned in the apicobasal direction.) These PAN-MTs could not be clearly identified by conventional immunofluorescence microscopy, which may explain why it was overlooked previously (Fig. 1 B).

Notably, soon after cell–cell adhesion was established, the PAN-MTs appeared as a separate network from the centrosomal MTs in the apicobasal view (Figs. 1 A and S1 A and Video 1). In contrast, long after cell–cell adhesion was established, centrosomes were located in the PAN-MT region, but they were no longer associated with MTs (Fig. S1 A and Video 2). Thus, the PAN-MTs form a noncentrosomal MT network that has not been previously described. In addition, we found the edges of the PAN-MTs associated with the cell–cell junction in a side-by-side fashion (Fig. 1 C). Next, to trace the ends of the PAN-MTs, we immunostained for α-tubulin, for EB1 as a plus-end marker of MTs and for Nezha as a minus-end marker of MTs. The minus and plus ends of MTs coexisted in the apical regions without any connections to centrosomes (Fig. S1 B and Video 3). Hence, the planar MTs are most likely noncentrosomal because they did not colocalize with centrosomes. This point remains to be further clarified in a future study.

Gel overlay assay for the association of MTs with TJ components

To evaluate the MT–TJ interaction, we performed a gel overlay assay of MTs (stabilized in their polymerized form by taxol) on polyvinylidene difluoride (PVDF) membranes, on which were blotted polypeptides from extracts of the epithelial cell–cell junction fraction isolated from liver (Tsukita and Tsukita, 1989; Furuse et al., 1993); this fraction contains a substantial amount of TJs. As shown in Fig. 1 D, the MTs showed strong binding to a 140-kD polypeptide (J-MAP 3, which was identified as cingulin by direct peptide sequencing) and weaker binding to three other bands (J-MAP 1, 2, and 4). We next asked whether cingulin mediated the MT–TJ interaction. In coprecipitation assays, α-tubulin was pulled down by anti-HA antibodies from HA-cingulin–overexpressing HEK293 cells, and an anti–α-tubulin antibody pulled down HA-cingulin (Fig. 2 A). Therefore, we identified cingulin as a MT-binding protein.

Domain analysis of cingulin's MT association

To examine the interaction between cingulin and MTs in more detail, we performed a domain analysis, in which we divided cingulin into three domains, a head domain (1–333 aa) and two rod domains, rod 1 (334–760 aa) and rod 2 (761–1,193 aa). The head domain of cingulin was previously reported to associate with actin, ZO-1, and ZO-2. On the other hand, two rod domains are coiled-coil regions that are involved in dimer formation (Citi et al., 2000; D'Atri et al., 2002). To examine the binding affinity of each domain to endogenous α-tubulin, we overexpressed the HA-tagged construct of full-length cingulin, or of the separate head, rod 1, or rod 2 domain, in HEK293 cells. The full-length and head domain of cingulin, but not the rod 1 or rod 2 domain, bound to α-tubulin, indicating that cingulin binds to MTs through its head domain (Fig. 2 B). It seemed that α-tubulin interacted better with the cingulin head domain than with the full length of cingulin, suggesting some conformational regulation of the binding between α-tubulin and cingulin in its full length, which was related to the phosphorylation of head domain of cingulin, as shown in Figs. 3 C and S3 B.

Furthermore, when the head domain of cingulin was divided into the subdomains of 1–202 aa and 203–333 aa, respectively, α-tubulin bound to the 1–202-aa sequence and ZO-1 to the 203–333-aa sequence, suggesting that the bindings of α-tubulin and ZO-1 to cingulin are not mutually exclusive (Fig. S1 C). Finally, we confirmed the binding between the proteins by using an endogenous coimmunoprecipitation assay; α-tubulin was pulled down by the anti-cingulin antibody, and an anti–α-tubulin antibody pulled down endogenous cingulin (Fig. 2 C).

The effect of cingulin KD on the association of TJs with MTs

We next asked whether cingulin mediated the side-by-side association of MTs with TJs. For this analysis, we generated cingulin KD Eph4 cells by the stable transfection of KD vectors (Fig. 2 D). Suppression of cingulin mRNA has no effect on AJ and TJ protein expression (Fig. S2 A), although immunofluorescence microscopy showed that the suppression of cingulin expression markedly decreased the side-by-side lateral association of MTs with TJs (Fig. 2 E). To exclude the possibility that the observed disruption was caused by a side effect of cingulin
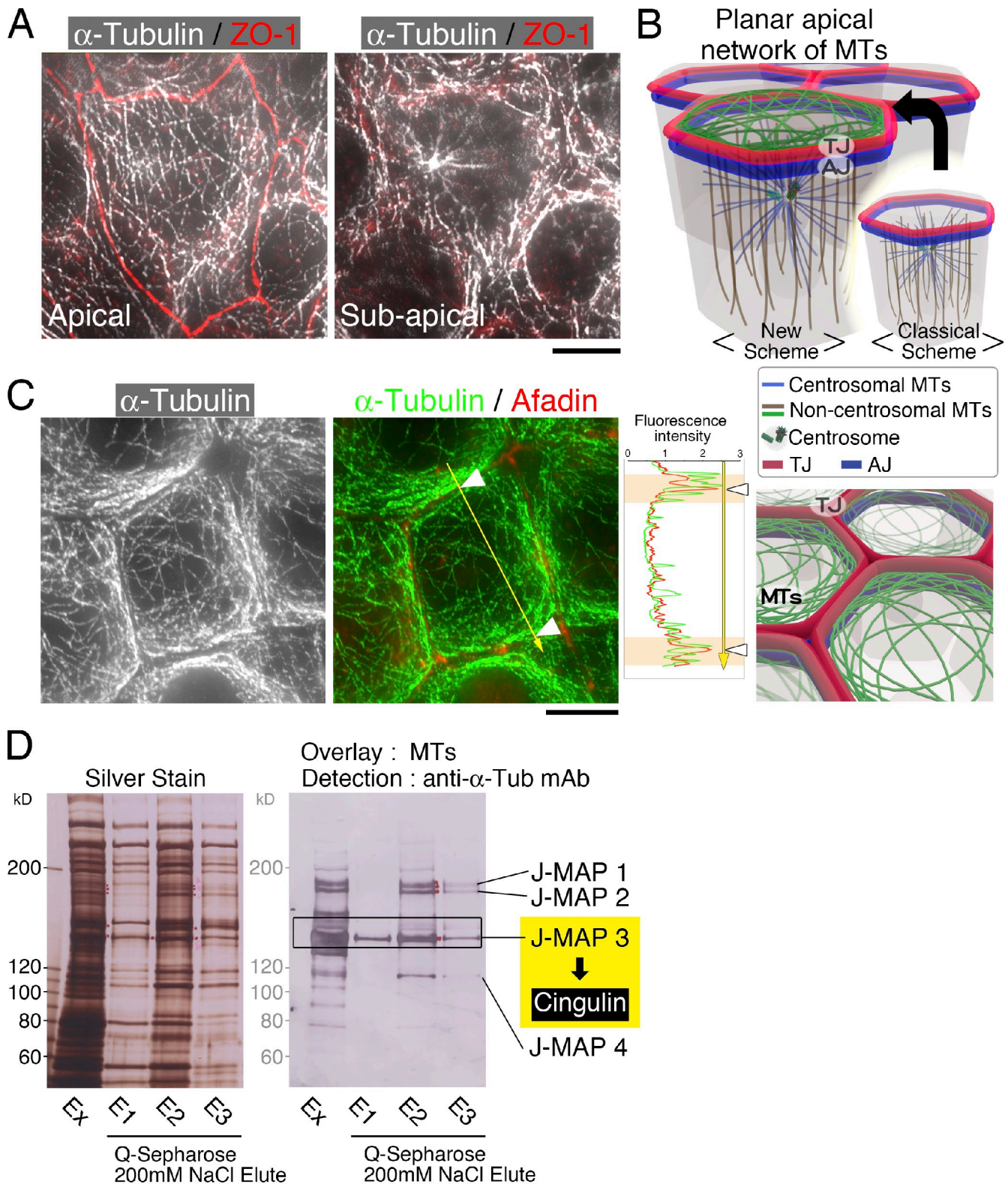
Figure 1. **PAN of noncentrosomal MTs associate with the cell–cell junction in a side-by-side fashion.** (A) SIM images of tubulin immunofluorescence in the apical and subapical planes of Eph4 cells. (B) Schematic drawing of the noncentrosomal MTs in epithelial cell sheets. In addition to the conventional noncentrosomal MTs, which are directed along the apicobasal axis, the PAN of noncentrosomal MTs appeared in the most apical plane of epithelial cell sheets. (C) SIM images of tubulin immunofluorescence in Eph4 cells. The planar apical noncentrosomal MTs are laterally associated with the cell–cell adhering junctions. The relative signal intensity of immunofluorescence was quantified along the yellow arrow for α-tubulin and afadin, respectively. In the orange color zone, α-tubulin was stacked on both sides of afadin-positive cell–cell contact regions (arrowheads). (D) Gel overlay analysis of cell–cell adhering junction components that bind MTs. Ex, eluate of buffer A containing 150 mM NaCl from BC-derived fraction applied SP Sepharose. E1, E2, and E3, fractions 1, 2, and 3 eluted by buffer A containing 200 mM NaCl from Ex applied Q Sepharose. α-Tub, α-tubulin. Bars, 5 µm.
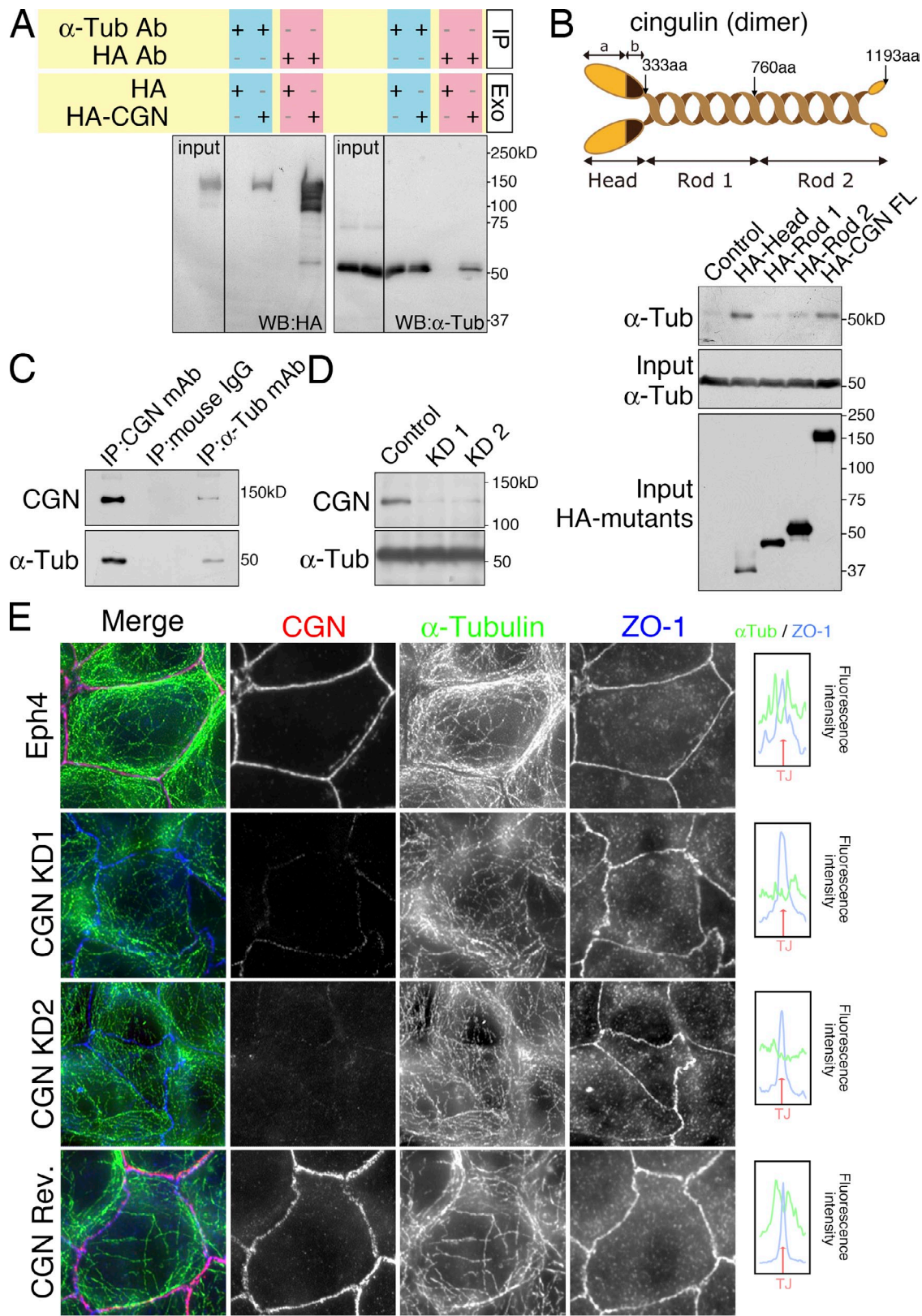
Figure 2. **Association of cingulin with α-tubulin.** (A) Coimmunoprecipitation of cingulin with α-tubulin. HA-cingulin (HA-CGN) or HA (HA) was exogenously overexpressed in HEK293 cells (Exo, exogenous), and their extracts were pulled down with an anti–α-tubulin antibody (α-Tub Ab). Black lines indicate that intervening lanes have been spliced out. IP, immunoprecipitation; WB, Western blotting. (B) Cingulin domain analysis for its association with α-tubulin. α-Tubulin binds to the head domain of cingulin. FL, full length. (C) Coimmunoprecipitation of endogenous cingulin with α-tubulin. Eph4 extracts were pulled down with anti-cingulin or anti–α-tubulin antibody. (D) Generation of cingulin knockdown (KD) Eph4 cells. (E) Immunofluorescence for α-tubulin in wild type, cingulin KD cells, and KD cells expressing an exogenous RNAi-resistant cingulin sequence (cingulin revertant [CGN] Rev.). Bar, 5 µm. The relative signal intensity of immunofluorescence was quantified for α-tubulin (top line) and ZO-1 (bottom line) for 10 cells.

KD, RNAi-resistant cingulin was transfected into cingulin KD cells, which restored the MT–TJ association. In addition, the MT–TJ association was disrupted in ZO-1 knockout Eph4 cells, in which cingulin is known to be dissociated from TJs (Fig. S1 D; Umeda et al., 2004). These findings collectively indicated that cingulin plays a major role in the side-by-side association of MTs with TJs. To examine the dynamics of the PAN-MTs, we transfected RFP-EB1 into Eph4 and cingulin KD cells, to trace the EB1 signals as the plus-end marker of MTs. In Eph4 cells, the EB1 signals were located parallel to the TJs. On the other hand, in cingulin KD cells, EB1 signals tended to be located end on with respect to the membranes at points of cell–cell adhesion (Videos 4 and 5).

Cingulin is also reported to associate with actin filaments (D'Atri and Citi, 2001) as well as with guanine nucleotide exchange factor (GEF)–H1 and p114 RhoGEF, as shown in MDCK and Caco-2 cells, respectively (Aijaz et al., 2005; Terry et al., 2011). There was no difference in actin filament arrangement, myosin light chain phosphorylation, p114 RhoGEF, or GEF-H1 between wild-type Eph4 and cingulin KD Eph4 cells (Fig. S2, B–E). We also did not detect differences in Rho activity, as shown in fluorescence resonance energy transfer (FRET) analyses, between the wild-type and cingulin KD cells (Videos 6 and 7). These results collectively indicated that cingulin mediates the lateral association of MTs with TJs, in a manner that does not involve Rho-related signaling.

Role of AMPK-mediated phosphorylation of cingulin in its association with MTs

We next examined the mechanism regulating cingulin's association with TJs. Cingulin is phosphorylated on its serine residues, similar to other TJ proteins, such as occludin and JAM-A (Citi and Denisenko, 1995; Seth et al., 2007; Raleigh et al., 2011; Iden et al., 2012). Cingulin has two AMPK target motifs L/SXXRXS/T at its serine-132 and -150 residues (Fig. 3 A), and TJ assembly is reported to be facilitated by the AMPK activator AICAR (5-aminoimidazole-4-carboxamide ribonucleotide; Zhang et al., 2006; Zheng and Cantley, 2007). We therefore examined whether cingulin is a substrate of AMPK. We first analyzed the binding of AMPK to cingulin, by coimmunoprecipitation experiments with exogenous HA-cingulin and V5-AMPKα1 expressed in HEK293 cells. The results showed that both proteins were coimmunoprecipitated by an anti-HA antibody, indicating that they bound each other (Fig. 3 B).

Next, to examine whether cingulin was a substrate of AMPK, we generated dephosphomimetic mutants of GST-cingulin, consisting of single (S132A or S150A) and double (S132A/S150A) dephosphomimetic mutants of cingulin fused to GST. GST-cingulin (wild type) and its dephosphomimetic mutants were purified and incubated with GST-AMPK (α1/β1/γ1) in the presence of ATP and AMP. The phosphorylation signals in the GST-cingulins were then examined using Pro-Q diamond, which detects phosphorylated proteins. Signals were detected in the bands of GST–wild-type cingulin, weaker signals were detected in the single mutant of S132A or S150A, and almost no signal was detected in the double dephosphomimetic mutant S132A/S150A (Fig. 3 C). Thus, cingulin is probably a phosphorylation substrate of AMPK, and S132 and S150 are AMPK's target sites.

We then examined the effects of the AMPK inhibitor compound C on cingulin's association with MTs in Eph4 cells. Immunofluorescence microscopy showed that the AMPK inhibitor affected the association of MTs with TJs, much as observed in cingulin KD cells, but not the localization of cingulin (Fig. 3 D). These results suggested that cingulin's function in mediating the MT–TJ association was regulated by its phosphorylation by AMPK. To further define the role of cingulin in the formation of the planar MT network, we examined calcium-switched formation of TJs. Because KD of cingulin and AMPK inhibitor induced detachment of the PAN-MTs from TJs, but did not affect the number of MTs in the apical network, it was likely that cingulin contributed to the stabilization of the MT–TJ interaction but not to the formation of the apical network of MTs (Fig. S3 A).

We addressed whether AMPK-mediated phosphorylation regulated cingulin's binding to MTs. For this purpose, lysates prepared from transfectants of HA-tagged wild-type cingulin or its dephosphomimetic mutants (S132A, S150A, and/or S132A/S150A) were immunoprecipitated with anti–α-tubulin. HA signals were detected in the wild-type cingulin bands, weaker signals were detected in the cingulin S132A or S150A bands, and almost no signal was detected in the double dephosphomimetic mutant S132A/S150A bands (Fig. 4 A). These findings supported the idea that the AMPK-mediated phosphorylation of cingulin regulated its binding to α-tubulin. Because compound C did not decrease the binding of α-tubulin with the head domain of cingulin, it was most likely that AMPK phosphorylation induced some conformational changes in cingulin to expose its binding sites to α-tubulin. Further studies are required to confirm this point (Fig. S3 B).

Next, we examined whether the AMPK-mediated phosphorylation of cingulin regulated the lateral interaction of MTs with TJs. The single or double phosphorylation site mutants localized to TJs but could not rescue the defective MT–TJ arrangement caused by cingulin KD (Fig. 4 B), and the double phosphomimetic mutant S132D/S150D rescued the MT–TJ arrangement caused by cingulin KD and inhibition of AMPK (Fig. S3 C). Taken with the finding that AMPK-mediated phosphorylation was the major phosphorylation in cingulin, it appears to play a critical role in cingulin's association with MTs, which is the basis of the interaction of MTs with TJs.

Role of the MT–TJ interaction in epithelial 3D morphogenesis

Finally, we examined the biological relevance of the MT–TJ association in epithelial cells. For this analysis, we performed 3D cultures of the following Eph4 cells: wild-type, cingulin KD, cingulin KD revertant expressing RNAi-resistant cingulin, and cingulin KD expressing cingulin dephosphomimetic mutants, in collagen IA gel. When the shape of the colonies was analyzed using ImageJ software, the colonies of wild-type Eph4 cells formed isotropic spheroids without lumen (Figs. 4 C and S3 D). In contrast, the colonies of cingulin KD cells had a distorted, anisotropic shape (Fig. 4 C). The cingulin KD revertant colonies showed the same round shape as the wild-type cells, indicating that the KD of cingulin was the direct cause of the deformation of the 3D Eph4 colonies (Fig. 4 C). Finally, when cingulin
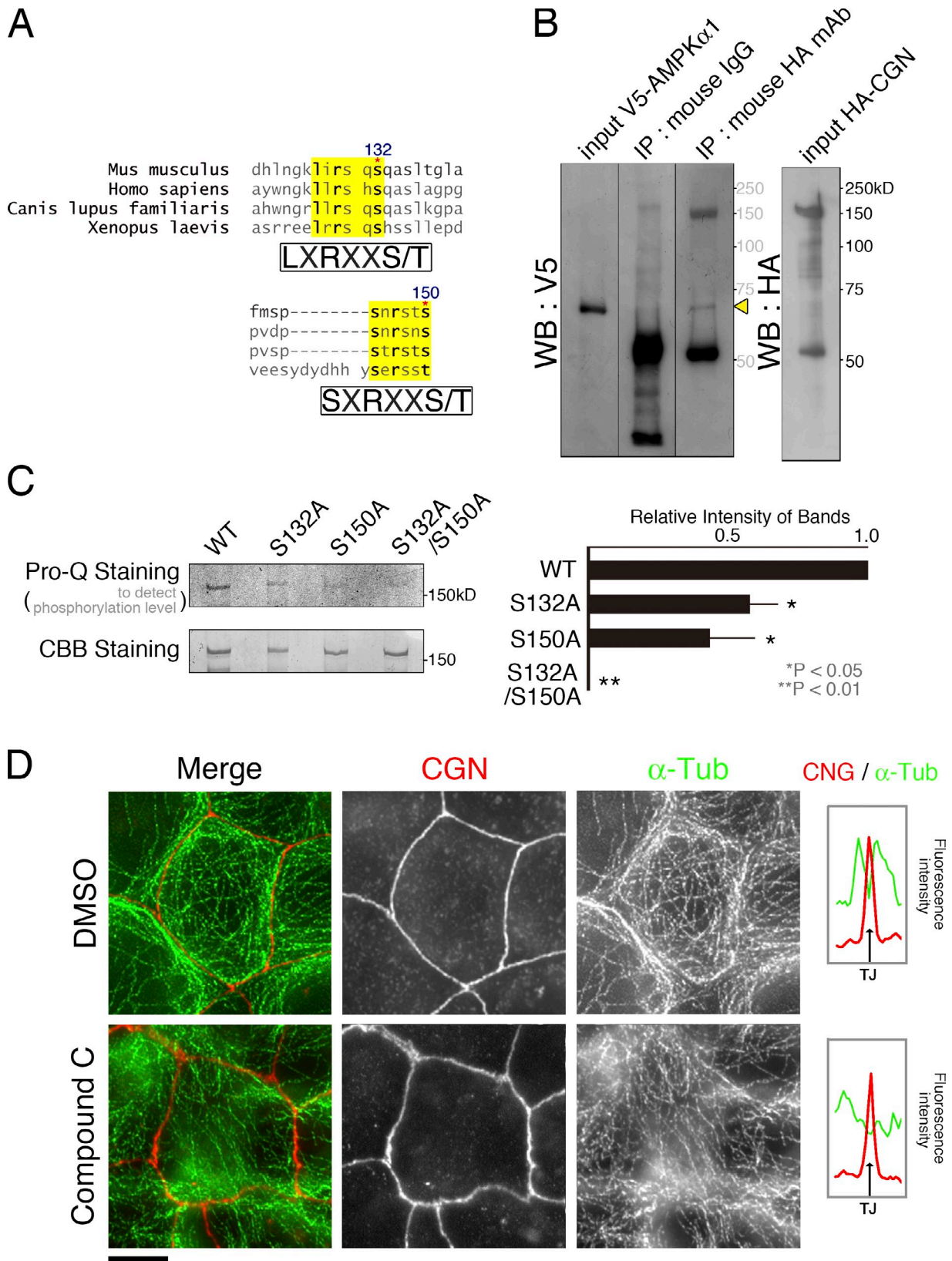
Figure 3. **Role of AMPK-mediated phosphorylation of cingulin in its association with MTs.** (A) AMPK target motifs in cingulin sequences (yellow shadowing). (B) Coimmunoprecipitation of HA-cingulin with V5-AMPKα1. Binding occurs between cingulin and AMPKα1 (yellow arrowhead, V5-AMPKα1). Black lines indicate that intervening lanes have been spliced out. WB, Western blot. (C) Phosphorylation level of wild-type and dephosphomimetic mutants of cingulin. As to the relative intensity, the ratio of intensity of Pro-Q staining to Coomassie brilliant blue (CBB) staining in wild type (WT) was normalized to 1.0, and the results are expressed as means ± SE (error bars; n = 3). (D) SIM images of the immunofluorescence in Eph4 cells treated with the AMPK inhibitor compound C. Bar, 5 µm. The α-tubulin association with TJs was disturbed by the AMPK inhibitor compound C. The relative signal intensity of immunofluorescence was quantified for α-tubulin (top line) and cingulin (bottom line) for 10 cells. CGN, cingulin; α-Tub, α-tubulin.
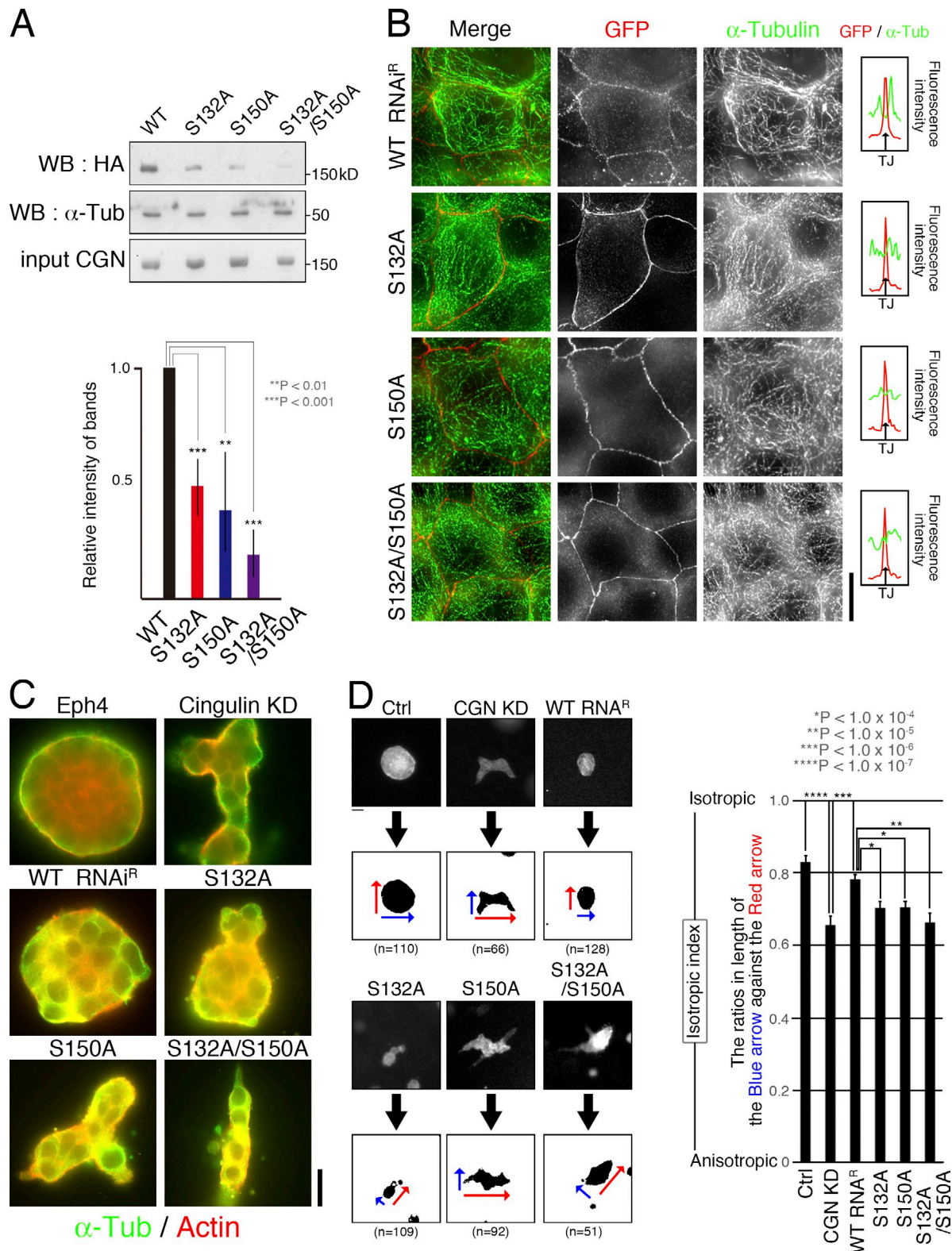
Figure 4.   **The AMPK phosphorylation on serines 132 and 150 of cingulin regulates its binding to α-tubulin and epithelial morphogenesis.** (A) Coimmuno-precipitation of exogenously expressed wild-type and dephosphomimetic cingulin with endogenous α-tubulin. As to the relative intensity, the band of wild type (WT) was normalized to 1.0, and the results are expressed as means ± SE (error bars; n = 3). WB, Western blot; α-Tub, α-tubulin; CGN, cingulin. (B) SIM images of tubulin immunofluorescence in cingulin KD cells in which wild-type or dephosphomimetic mutants of cingulin were expressed. The relative signal intensity of immunofluorescence was quantified for α-tubulin and GFP for 10 cells. (C) Epithelial morphogenesis in 3D culture in collagen IA gel of control and cingulin KD cells with or without the expression of wild-type or dephosphomimetic cingulin. (D) Quantification of the isotropy or anisotropy of the colonies of control and cingulin KD Eph4 cells with or without the expression of wild-type or dephosphomimetic cingulin. The ratio of the shortest length (blue arrow) to that of the longest (red arrow) of the Eph4 cell colonies was determined as the isotropic index. The results are expressed as means ± SE (error bars) as quantified from three independent experiments. Ctrl, control. Bars: (B) 10 μm; (C and D) 20 μm.

Figure 5. **Schematic drawing of the MT–TJ side-by-side interaction occurring via cingulin and regulated by cingulin's phosphorylation by AMPK.** Schematic drawing of the suggested mechanism for the regulation of the lateral association of MTs with TJs. In the TJs in the apical plane of the epithelial cell sheets, cingulin is anchored to claudin by ZO-1. When cingulin is phosphorylated by AMPK, it binds MTs and mediates their association with TJs.
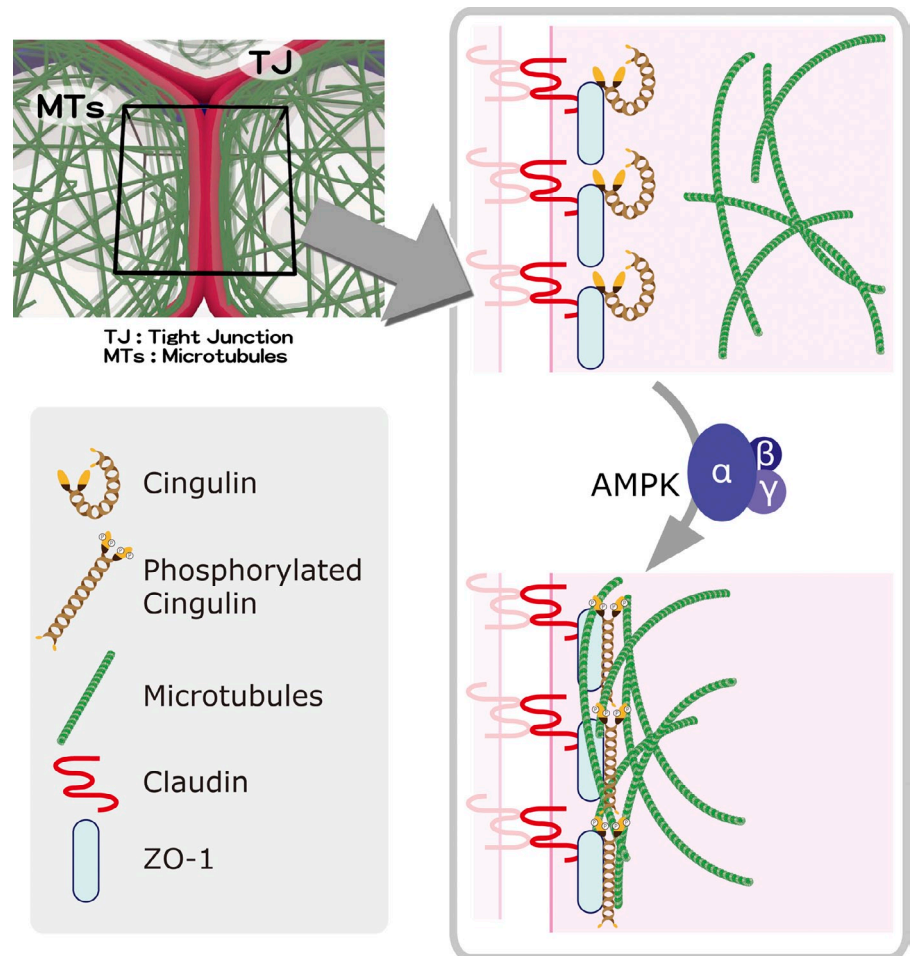
dephosphomimetic mutants were expressed in cingulin KD cells, the colonies showed a distorted, anisotropic shape, indicating that phosphorylation of cingulin is critical for the shape of colonies.

We quantified the isotropies of the 3D colonies by representing the colonies as rectangles and determining the isotropic indexes as the ratios of the shortest to the longest lengths. This ratio was significantly different between the 3D colonies of wild-type and cingulin KD cells, 0.83 ± 0.017 ($n = 110$) and 0.65 ± 0.026 ($n = 66$), respectively. The ratio in the revertant was 0.78 ± 0.008 ($n = 128$). Furthermore, branching of the 3D colonies of cingulin KD cells occurred but was not seen in the colonies of wild-type or cingulin KD revertant cells (Fig. 4 D). The expression of phosphomimetic mutants does not significantly show such effects. In addition, Eph4 cells treated with compound C formed the anisotropic colony (0.59 ± 0.012, $n = 302$; Fig. S3 E). Thus, anisotropy and branching were induced by the absence or dephosphorylation of cingulin. These findings indicated that the AMPK-mediated MT–TJ interaction probably contributes to epithelial morphogenesis, and the apical MT network provides sufficient tension to the apical membrane to form the isotropic spherical shape, pointing to a critical role of the apical configuration of epithelial cell sheets.

Conclusion

In summary, as schematically shown in Fig. 5, we have for the first time revealed a PAN of noncentrosomal MTs (PAN-MTs),

which is laterally associated with the TJs through cingulin, in its AMPK-phosphorylated form, by the high-contrast images achieved by SIM. AMPK is a kinase that plays critical roles in the regulation of a wide spectrum of metabolic homeostasis and is reported to generate a variety of biological cues (Leprivier et al., 2013; Miller et al., 2013; O'Neill and Hardie, 2013). This kinase regulates energy-dependent processes in epithelial morphogenesis, cell polarity, and tumor suppression (Lo et al., 2012; Martin-Belmonte and Perez-Moreno, 2012). In this respect, the PAN-MT system is a target of metabolic homeostasis-related AMPK regulation, involved in the apical maturation of epithelial cell sheets and epithelial morphogenesis. These findings increase our basic understanding not only of epithelial cell biology but also of cancer and developmental biology.

Materials and methods

Reagents

Primary antibodies used in this work were mouse anti–α-tubulin mAb (Sigma-Aldrich), rat anti–α-tubulin mAb (Abcam), mouse anti-HA mAb (Covance), rat anti-HA mAb (Roche), and rat anti-GFP mAb (Nacalai Tesque) antibodies. Mouse Anti-V5 mAb (Invitrogen) was gifted by S. Takashima and O. Tsukamoto (Osaka University, Osaka, Japan) and mouse anti-cingulin mAb (antigen: full-length of cingulin) was produced by K. Owaribe (Nagoya University, Nagoya, Japan). Rabbit anti–ZO-1 pAb (antigen: F4 fragment including 30–340 aa; Itoh et al., 1993) and mouse anti-afadin mAb (antigen: full-length of afadin) were generated in our laboratory. Alexa Flour 488–, 568–, and 647–labeled secondary antibodies and rhodamine-conjugated

phalloidin were commercially obtained (Invitrogen). HRP-conjugated secondary antibodies were also commercially obtained (BD). Compound C was commercially obtained (EMD Millipore).

KD constructs
To suppress the expression of cingulin in Eph4 cells, oligonucleotides of target sequence were cloned into the H1 promoter-driven RNAi vector (Brummelkamp et al., 2002). The vector was transfected and suppressed the expression of cingulin, and we obtained two clones. The probe sequence was cingulin, 5'-GACCGTTTGTGGTTCTTAAC-3'.

Cell culture and transfection
Mouse Eph4 epithelial cells, cingulin KD cells, and HEK293 cells were grown in Dulbecco's modified Eagle's medium supplemented with 10% fetal calf serum. Transfection was performed using Lipofectamine Plus reagent (Invitrogen) according to the manufacturer's instructions.

Immunofluorescence microscopy
Cells were fixed in cold methanol for 10 min on ice or fixed in 1% formalin for 5 min at RT followed by treatment with 0.1% Triton X-100 in PBS. After blocking for 10 min, cells were incubated with primary antibodies in blocking buffer for 1 h at RT or overnight at 4°C. After washing, cells were incubated with fluorochrome-conjugated secondary antibodies for 1 h at RT. The cells were mounted in fluorescence mounting medium (Dako). The specimens were observed with a photomicroscopy (BX51 and BX70; Olympus) equipped with a 100×, 1.4 NA oil immersion lens, 60×, 1.42 NA oil immersion lens, and 20×, 0.5 NA lens, and with a superresolution SIM (ELYRA S.1; Carl Zeiss) equipped with a Plan Apochromat (100×, 1.46 NA oil immersion lens, 63×, 1.4 NA oil immersion lens, and 40×, 1.4 NA oil immersion lens) with appropriate binning of pixels and exposure time. Photographs were recorded with a cooled charge-coupled device camera (ORCA-ER [Hamamatsu Photonics] or CoolSNAP HQ [Photometrics]). The images were analyzed with MetaMorph (Molecular Devices) or ZEN (Carl Zeiss).

Gel overlay assay
The junctional fraction was prepared from the liver of newly hatched or 2-d-old chicks through the crude membrane and the bile canaliculi (BC) fractions according to the method described previously (Tsukita and Tsukita, 1989). The BC fraction was diluted fivefold (vol/vol) with hypotonic buffer (1 mM NaHCO$_3$ and 2 µg/ml leupeptin, pH 7.5) and centrifuged at 100,000 g for 30 min at 4°C. The precipitate was dissolved with buffer A (50 mM Hepes, pH 7.5, 1 mM EGTA, 6 M urea, 2 µg/ml leupeptin, and 10 mM APMSF) and centrifuged at 100,000 g for 60 min at 4°C. The resulting supernatant (∼20 mg) was applied to an SP Sepharose column (GE Healthcare). After the column was washed with buffer A containing 50 mM NaCl, the binding proteins were eluted with the same buffer containing 100 mM NaCl and then with buffer A containing 150 mM NaCl. The eluate from the 150 mM NaCl solution was diluted threefold with buffer A and applied to a Q Sepharose column (GE Healthcare). The column was washed with buffer A containing 150 mM NaCl, and bound proteins were then eluted with the same buffer containing 200 mM NaCl. Aliquots of the eluate were subjected to SDS-PAGE (4–7.5% gradient gel) and transferred to the PVDF membrane.

Pig brain tubulin was purified as previously described (Nishida et al., 1987). Purified tubulin (∼1 mg/ml) was polymerized into MTs by incubating for 60 min at 37°C in 3 mM MgCl$_2$, 1 mM EGTA, 1 mM GTP, 10% DMSO, and 80 mM Pipes, pH 6.8. The sample was then diluted 22-fold in PME buffer (1 mM MgCl$_2$, 1 mM EGTA, 20 µM taxol, and 80 mM Pipes, pH 6.8) and kept at RT.

The PVDF membrane was blocked with 5% skim milk (Megmilk Snow Brand Co., Ltd.) in PME buffer for 1 h at RT. The membrane was then incubated with 5% skim milk in PME buffer, which contains 45 µg/ml of MTs, for 2 h at 37°C. After washing with PME buffer for 5 min at 37°C three times, the bound polymerized tubulin was detected using an anti–α-tubulin antibody.

Immunoprecipitation
HEK293 cells were transfected with expression vectors. Cell lysates were incubated with protein A–Sepharose bound with the anti–α-tubulin or anti-HA antibody. Immune complexes were fully washed and then resuspended in 30 µl SDS sample buffer, and 5- and 20-µl aliquots of each were analyzed by Western blotting.

Western blotting
To prepare total cell lysates for immunoblotting, Eph4 or HEK293 cells were lysed with SDS-PAGE sample buffer, sonicated, and boiled. The protein samples were separated by SDS-PAGE, transferred onto a nitrocellulose or PVDF membrane, and blotted with the appropriate antibodies. For quantification of signals in Western blotting, the densitometric quantification of immunoblot bands with loading control in the same immunoblotting membranes was performed using ImageJ software (National Institutes of Health).

Cingulin phosphorylation assay
Cingulin phosphorylation assays were performed at 30°C in a reaction volume of 30 µl containing 20 mM Tris-HCl, pH 7.4, 0.3 mM NaCl, 0.2 mM AMP, 0.8 mM MgCl$_2$, and 0.2 mM ATP, containing 0.1 mM recombinant AMPKα1/β1/γ1 (Carna Biosciences) and either of 1 µg GST-cingulin or GST-cingulin mutants. After 90 min, reactions were terminated by the addition of SDS solution. These samples were separated by SDS-PAGE. The gels were stained with Pro-Q diamond (Invitrogen) according to the manufacturer's instructions, and the phosphorylation signals were detected by a scanner (Typhoon 9200; GE Healthcare). Densitometric quantification of phosphorylation bands was performed using ImageJ software.

3D culture
Cells were added to a collagen I (Nitta Gelatin) mixture, gently mixed, and plated onto 12-well transwell insert plates at 5×10^4 cells/well. 3 d after plating, cysts were examined for the immunofluorescence microscopy (Yano et al., 2011). After treatment with collagenase III (Sigma-Aldrich), cells were fixed in cold methanol for 30 min on ice or fixed in 1% formalin for 30 min at RT followed by treatment with 0.1% Triton X-100 in PBS. After blocking for 30 min, cells were incubated with primary antibodies in blocking buffer overnight at 4°C. After washing, cells were incubated with Alexa Flour 488–, 568–, and 647–labeled secondary antibodies for 3 h at RT. Cells were mounted in fluorescence mounting medium (Dako). The specimens were observed with a superresolution SIM (ELYRA S.1) or confocal microscope (LSM 510; Carl Zeiss) equipped with a Plan Apochromat (100×, 1.46 NA oil immersion lens, 63×, 1.4 NA oil immersion lens, and 40×, 1.4 NA oil immersion lens) with appropriate binning of pixels and exposure time. The images were analyzed with ZEN or LSM 510 Meta version 3.0 (Carl Zeiss).

Imaging analysis
By using ImageJ, an image processing software, we quantified the isotropies of the 3D colonies by representing the colonies as rectangles and determining the isotropic indexes as the ratios of the shortest to the longest lengths.

Statistical analysis
Data are presented as means ± SE. Whenever necessary, statistical significance of the data was analyzed by performing one-sample t tests. The specific types of tests and the p-values, when applicable, are indicated in the figures.

Online supplemental material
Fig. S1 shows additional data on the MTs associated with TJs and additional data on the head domain of cingulin. Fig. S2 shows the characterization of cingulin KD cells. Fig. S3 shows the effect of AMPK inhibitor and phosphorylation of head domain of cingulin on MTs arrangements. Video 1 shows the PAN-MTs of Eph4 cells 48 h after being seeded. Video 2 shows the PAN-MTs of Eph4 cells 72 h after being seeded. Video 3 shows the side-by-side association of the PAN-MTs with TJs in an Eph4 cell. Video 4 shows the dynamics of the PAN-MTs in Eph4 cells. Video 5 shows the dynamics in the PAN-MTs of cingulin KD Eph4 cells. Video 6 shows FRET analysis for Raichu-RhoA in the Eph4 cells during 12 and 24 h after Ca^{2+} switch. Video 7 shows FRET analysis for Raichu-RhoA in the cingulin KD Eph4 cells during 12 and 24 h after Ca^{2+} switch. Online supplemental material is available at http://www.jcb.org/cgi/content/full/jcb.201304194/DC1.

References

Aijaz, S., F. D'Atri, S. Citi, M.S. Balda, and K. Matter. 2005. Binding of GEF-H1 to the tight junction-associated adaptor cingulin results in inhibition of Rho signaling and G1/S phase transition. *Dev. Cell*. 8:777–786. http://dx.doi.org/10.1016/j.devcel.2005.03.003

Bacallao, R., C. Antony, C. Dotti, E. Karsenti, E.H. Stelzer, and K. Simons. 1989. The subcellular organization of Madin–Darby canine kidney cells during the formation of a polarized epithelium. *J. Cell Biol.* 109:2817–2832. http://dx.doi.org/10.1083/jcb.109.6.2817

Bartolini, F., and G.G. Gundersen. 2006. Generation of noncentrosomal microtubule arrays. *J. Cell Sci.* 119:4155–4163. http://dx.doi.org/10.1242/jcs.03227

Baum, B., and M. Georgiou. 2011. Dynamics of adherens junctions in epithelial establishment, maintenance, and remodeling. *J. Cell Biol.* 192:907–917. http://dx.doi.org/10.1083/jcb.201009141

Bornslaeger, E.A., C.M. Corcoran, T.S. Stappenbeck, and K.J. Green. 1996. Breaking the connection: displacement of the desmosomal plaque protein desmoplakin from cell–cell interfaces disrupts anchorage of intermediate filament bundles and alters intercellular junction assembly. *J. Cell Biol.* 134:985–1001. http://dx.doi.org/10.1083/jcb.134.4.985

Brummelkamp, T.R., R. Bernards, and R. Agami. 2002. A system for stable expression of short interfering RNAs in mammalian cells. *Science*. 296:550–553. http://dx.doi.org/10.1126/science.1068999

Citi, S., and N. Denisenko. 1995. Phosphorylation of the tight junction protein cingulin and the effects of protein kinase inhibitors and activators in MDCK epithelial cells. *J. Cell Sci.* 108:2917–2926.

Citi, S., F. D'Atri, and D.A. Parry. 2000. Human and *Xenopus* cingulin share a modular organization of the coiled-coil rod domain: predictions for intra- and intermolecular assembly. *J. Struct. Biol.* 131:135–145. http://dx.doi.org/10.1006/jsbi.2000.4284

D'Atri, F., and S. Citi. 2001. Cingulin interacts with F-actin in vitro. *FEBS Lett.* 507:21–24. http://dx.doi.org/10.1016/S0014-5793(01)02936-2

D'Atri, F., F. Nadalutti, and S. Citi. 2002. Evidence for a functional interaction between cingulin and ZO-1 in cultured cells. *J. Biol. Chem.* 277:27757–27764. http://dx.doi.org/10.1074/jbc.M203717200

Etienne-Manneville, S., and A. Hall. 2002. Rho GTPases in cell biology. *Nature*. 420:629–635. http://dx.doi.org/10.1038/nature01148

Franke, W.W. 2009. Discovering the molecular components of intercellular junctions—a historical view. *Cold Spring Harb. Perspect. Biol.* 1:a003061. http://dx.doi.org/10.1101/cshperspect.a003061

Furuse, M., T. Hirase, M. Itoh, A. Nagafuchi, S. Yonemura, S. Tsukita, and S. Tsukita. 1993. Occludin: a novel integral membrane protein localizing at tight junctions. *J. Cell Biol.* 123:1777–1788. http://dx.doi.org/10.1083/jcb.123.6.1777

Gumbiner, B.M. 2000. Regulation of cadherin adhesive activity. *J. Cell Biol.* 148:399–404. http://dx.doi.org/10.1083/jcb.148.3.399

Iden, S., S. Misselwitz, S.S. Peddibhotla, H. Tuncay, D. Rehder, V. Gerke, H. Robenek, A. Suzuki, and K. Ebnet. 2012. aPKC phosphorylates JAM-A at Ser285 to promote cell contact maturation and tight junction formation. *J. Cell Biol.* 196:623–639. http://dx.doi.org/10.1083/jcb.201104143

Itoh, M., A. Nagafuchi, S. Yonemura, T. Kitani-Yasuda, S. Tsukita, and S. Tsukita. 1993. The 220-kD protein colocalizing with cadherins in non-epithelial cells is identical to ZO-1, a tight junction–associated protein in epithelial cells: cDNA cloning and immunoelectron microscopy. *J. Cell Biol.* 121:491–502. http://dx.doi.org/10.1083/jcb.121.3.491

Leprivier, G., M. Remke, B. Rotblat, A. Dubuc, A.R. Mateo, M. Kool, S. Agnihotri, A. El-Naggar, B. Yu, S.P. Somasekharan, et al. 2013. The eEF2 kinase confers resistance to nutrient deprivation by blocking translation elongation. *Cell*. 153:1064–1079. http://dx.doi.org/10.1016/j.cell.2013.04.055

Lo, B., G. Strasser, M. Sagolla, C.D. Austin, M. Junttila, and I. Mellman. 2012. Lkb1 regulates organogenesis and early oncogenesis along AMPK-dependent and -independent pathways. *J. Cell Biol.* 199:1117–1130. http://dx.doi.org/10.1083/jcb.201208080

Martin-Belmonte, F., and M. Perez-Moreno. 2012. Epithelial cell polarity, stem cells and cancer. *Nat. Rev. Cancer.* 12:23–38. http://dx.doi.org/10.1038/nrc3169

Meng, W., and M. Takeichi. 2009. Adherens junction: molecular architecture and regulation. *Cold Spring Harb. Perspect. Biol.* 1:a002899. http://dx.doi.org/10.1101/cshperspect.a002899

Meng, W., Y. Mushika, T. Ichii, and M. Takeichi. 2008. Anchorage of microtubule minus ends to adherens junctions regulates epithelial cell-cell contacts. *Cell*. 135:948–959. http://dx.doi.org/10.1016/j.cell.2008.09.040

Miller, R.A., Q. Chu, J. Xie, M. Foretz, B. Viollet, and M.J. Birnbaum. 2013. Biguanides suppress hepatic glucagon signalling by decreasing production of cyclic AMP. *Nature*. 494:256–260. http://dx.doi.org/10.1038/nature11808

Moss, D.K., G. Bellett, J.M. Carter, M. Liovic, J. Keynton, A.R. Prescott, E.B. Lane, and M.M. Mogensen. 2007. Ninein is released from the centrosome and moves bi-directionally along microtubules. *J. Cell Sci.* 120:3064–3074. http://dx.doi.org/10.1242/jcs.010322

Nishida, E., M. Hoshi, Y. Miyata, H. Sakai, T. Kadowaki, M. Kasuga, S. Saijo, H. Ogawara, and T. Akiyama. 1987. Tyrosine phosphorylation by the epidermal growth factor receptor kinase induces functional alterations in microtubule-associated protein 2. *J. Biol. Chem.* 262:16200–16204.

O'Neill, L.A., and D.G. Hardie. 2013. Metabolism of inflammation limited by AMPK and pseudo-starvation. *Nature*. 493:346–355. http://dx.doi.org/10.1038/nature11862

Perez-Moreno, M., C. Jamora, and E. Fuchs. 2003. Sticky business: orchestrating cellular signals at adherens junctions. *Cell*. 112:535–548. http://dx.doi.org/10.1016/S0092-8674(03)00108-9

Raleigh, D.R., D.M. Boe, D. Yu, C.R. Weber, A.M. Marchiando, E.M. Bradford, Y. Wang, L. Wu, E.E. Schneeberger, L. Shen, and J.R. Turner. 2011. Occludin S408 phosphorylation regulates tight junction protein interactions and barrier function. *J. Cell Biol.* 193:565–582. http://dx.doi.org/10.1083/jcb.201010065

Reinsch, S., and E. Karsenti. 1994. Orientation of spindle axis and distribution of plasma membrane proteins during cell division in polarized MDCKII cells. *J. Cell Biol.* 126:1509–1526. http://dx.doi.org/10.1083/jcb.126.6.1509

Seth, A., P. Sheth, B.C. Elias, and R. Rao. 2007. Protein phosphatases 2A and 1 interact with occludin and negatively regulate the assembly of tight junctions in the CACO-2 cell monolayer. *J. Biol. Chem.* 282:11487–11498. http://dx.doi.org/10.1074/jbc.M610597200

Shaw, R.M., A.J. Fay, M.A. Puthenveedu, M. von Zastrow, Y.N. Jan, and L.Y. Jan. 2007. Microtubule plus-end-tracking proteins target gap junctions directly from the cell interior to adherens junctions. *Cell*. 128:547–560. http://dx.doi.org/10.1016/j.cell.2006.12.037

Sugimoto, M., A. Inoko, T. Shiromizu, M. Nakayama, P. Zou, S. Yonemura, Y. Hayashi, I. Izawa, M. Sasoh, Y. Uji, et al. 2008. The keratin-binding protein Albatross regulates polarization of epithelial cells. *J. Cell Biol.* 183:19–28. http://dx.doi.org/10.1083/jcb.200803133

Terry, S.J., C. Zihni, A. Elbediwy, E. Vitiello, I.V. Leefa Chong San, M.S. Balda, and K. Matter. 2011. Spatially restricted activation of RhoA signalling at epithelial junctions by p114RhoGEF drives junction formation and morphogenesis. *Nat. Cell Biol.* 13:159–166. http://dx.doi.org/10.1038/ncb2156

Tsukita, S., and S. Tsukita. 1989. Isolation of cell-to-cell adherens junctions from rat liver. *J. Cell Biol.* 108:31–41. http://dx.doi.org/10.1083/jcb.108.1.31

Tsukita, S., M. Furuse, and M. Itoh. 2001. Multifunctional strands in tight junctions. *Nat. Rev. Mol. Cell Biol.* 2:285–293. http://dx.doi.org/10.1038/35067088

Umeda, K., T. Matsui, M. Nakayama, K. Furuse, H. Sasaki, M. Furuse, and S. Tsukita. 2004. Establishment and characterization of cultured epithelial cells lacking expression of ZO-1. *J. Biol. Chem.* 279:44785–44794. http://dx.doi.org/10.1074/jbc.M406563200

Yano, T., Y. Yamazaki, M. Adachi, K. Okawa, P. Fort, M. Uji, S. Tsukita, and S. Tsukita. 2011. Tara up-regulates E-cadherin transcription by binding to the Trio RhoGEF and inhibiting Rac signaling. *J. Cell Biol.* 193:319–332. http://dx.doi.org/10.1083/jcb.201009100

Zhang, L., J. Li, L.H. Young, and M.J. Caplan. 2006. AMP-activated protein kinase regulates the assembly of epithelial tight junctions. *Proc. Natl. Acad. Sci. USA*. 103:17272–17277. http://dx.doi.org/10.1073/pnas.0608531103

Zheng, B., and L.C. Cantley. 2007. Regulation of epithelial tight junction assembly and disassembly by AMP-activated protein kinase. *Proc. Natl. Acad. Sci. USA*. 104:819–822. http://dx.doi.org/10.1073/pnas.0610157104